MOEM

Modern Electronic Materials 2024; 10(1): 51–57
DOI 10.3897/j.moem.10.1.130290

Research Article

Growth of thin-film magnetic nanostructures promising for spintronics applications

Andrey V. Telegin[1], Zhimba Zh. Namsaraev[2], Vladimir D. Bessonov[1], Valentin S. Teplov[1], Alexey V. Ognev[2,3]

1 *M.N. Mikheev Institute of Metal Physics of Ural Branch of Russian Academy of Sciences, 18 Sofia Kovalevskay Str., Ekaterinburg 620108, Russian Federation*

2 *Far Eastern Federal University, 10 Ajax Bay, Russky Island, Vladivostok 690922, Russian Federation*

3 *Sakhalin State University, 33 Kommunisticheskiy Ave., Yuzhno-Sakhalinsk 693000, Russian Federation*

Corresponding author: Andrey V. Telegin (telegin@imp.uran.ru)

Received 6 October 2023 ♦ **Accepted** 20 December 2023 ♦ **Published** 5 April 2024

Citation: Telegin AV, Namsaraev ZhZh, Bessonov VD, Teplov VS, Ognev AV (2024) Growth of thin-film magnetic nanostructures promising for spintronics applications. *Modern Electronic Materials* 10(1): 51–57. https://doi.org/10.3897/j.moem.10.1.130290

Abstract

Multilayered metallic nanostructures are promising for the fabrication of spin valves based on the giant magnetoresistive effect and for studies of the nature of topological magnetism, aimed at the development of new nanoscale data storage and transfer devices, e.g. those based on magnetic skyrmions. It is still an important task to develop methods of synthesis and configuration of thin-film nanostructures and control of spin textures in those nanostructures under electric and spin currents generated as a result of the spin Hall effect in external electric fields. Thin-film polycrystalline ferromagnetic / heavy metal Ru(10nm)/Co(0,8)/Ru(2), Ru(10)/Co(0,8)/Ru(2)/W(4), Pt(5)/Co(0,8)/MgO(2)/Pt(2) and Pt(15)/Co(0,8)/MgO(2)/Pt(2) nanostructures have been synthesized using magnetron sputtering. Electric contacts and Hall structures with different conductive bridge thicknesses have been synthesized on the specimens using electron beam photolithography. Experimental vibration magnetometric data have been utilized to calculate magnetic parameters of the specimens, i.e., saturation magnetization, magnetic anisotropy energy and field and coercive force as functions of ferromagnetic and heavy metal layer types. The domain structure of the specimens has been studied using Kerr microscopy. The electrical resistivity has been simulated and the critical current and current density of the nanostructures have been assessed. We show that all the film specimens exhibit perpendicular magnetic anisotropy and can be used in the studies of current-induced phenomena and spin moment transfer processes in nanostructures.

Keywords

magnetron sputtering, nanostructures, photolithography, Kerr microscopy, spintronics, perpendicular magnetic anisotropy, metallic films

1. Introduction

Multilayered films with ultrathin ferromagnetic metal layers exhibit unique magnetic and transport properties and have for a long time been attracting the attention of researchers due to the possibility of developing magnetic field sensing devices on their basis [1–3]. The synthesis of magnetic nanostructures requires understanding the processes occurring therein and the fundamental origins of their magnetic behavior, as well as high engineering capabilities and well-developed methods of synthesizing specimens with required functional properties.

For example, varying the nanostructure growth process and geometry, number and thickness of layers and substrate parameters, one can control the magnetostatic energy and effective magnetic anisotropy of the growing nanostructures and change the orientation of their easy and hard magnetization axes [4–10], finally obtaining the required mciromagnetic configuration and general magnetic behavior. Study of the domain structure and remagnetization mechanisms in magnetic nanostructures is also of practical interest. For example, the effect of domain boundary movement in nanomaterials is widely used for the development of new types of non-volatile magnetic memory and logical devices [11, 12]. Studies at the nexus of topological magnetism and spintronics (spin-orbitronics and skyrmionics) open new technological opportunities for the development of UHF and THz ultrafast nanoscale data transfer and processing devices with controlled losses and noise [13–15]. Thus, a fundamental task of spintronics and its new branch spin-orbitronics is to study the nature of topological magnetism in collinear and non-collinear spin systems with strong spin-orbit coupling, over the discovery of magnetic skyrmions that can be stabilized in ferromagnetic media at room temperature. The most interesting results were obtained for heavy metal (HM = Pt, W, Ta etc.) / ferromagnetic (FM = Co, CoFe etc.) metallic nanostructures having perpendicular anisotropy and strong Dzyaloshinskii–Moriya interaction [16–21]. An important task of spintronics is to develop methods of controlling the spin textures in thin-film HM/FM nanostructures affected by polarized and pure spin currents caused by the spin Hall effect in the HM layer and by external magnetic fields (e.g. UHF) for the goal-oriented generation of individual static and dynamic magnetic skyrmions [19–24]. However, despite the large number of publications on the topic it is still not completely clear which materials or structures are optimum for the practical applications in this field. Furthermore, studies of the transport properties and spin moment transfer processes in metallic nanostructures require complex-geometry specimens with various types of current contacts, e.g. Hall bridges, thus imposing limitations on the research capabilities.

Presented below are our new synthesis method and experimental results for synthesized and calibrated thin-film magnetic HM (Ru, Pt, W) / FM (Co) Hall contact nanostructures. The saturation magnetization, perpendicular magnetic anisotropy, domain structure and critical currents of the films were assessed based on the experimental Kerr microscopy, magnetic and electrical data. We show that the specimens can be used for studying spin transport properties.

2. Experimental

Polycrystalline films were synthesized on one side of polished thermally oxidized silicon substrates Si(675mm)/SiO_2(500nm) (Si-mat Co., Korea) in an Omicron ultrahigh-vacuum plant (Fig. 1*a*) equipped with four magnetron sputtering sources. The film compositions and layer thicknesses are presented below.

Specimen number	Composition
1	Ru(10nm)/Co(0.8nm)/Ru(2nm)
2	Ru(10nm)/Co(0.8nm)/Ru(2nm)/W(4nm)
3	Pt(5nm)/Co(0.8nm)/MgO(2nm)/Pt(2nm)
4	Pt(15nm)/Co(0.8nm)/MgO(2nm)/Pt(2nm)

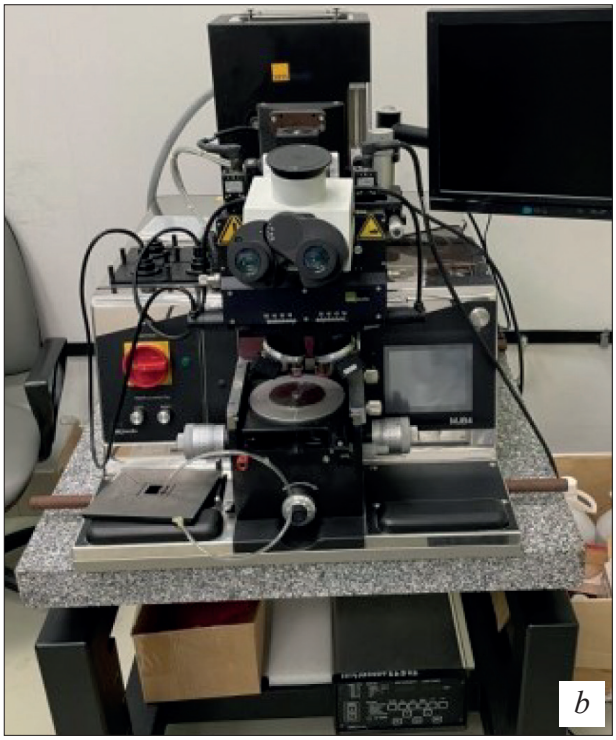

Figure 1. Nanostructure synthesis equipment: (*a*) Omicron ultrahigh-vacuum plant with four magnetron sputtering sources; (*b*) Suss Microtec MJB4 contact photolithography system

Specimen were placed on a rotating HM holder for the deposition of films having uniform and isotropic thicknesses and compositions. The base pressure in the chamber was $1.33 \cdot 10^{-6}$ Pa. Metallic layers (Pt, W, Co, Ru) were sputtered in direct current (DC) mode at an Ar gas pressure of 0.4 Pa and a 22 W power. The deposition rates were monitored for different layers with a quartz thickness gage: V_{Pt} = 0.05 nm/s, V_{MgO} = 0.02 nm/s, V_W = 0.015 nm/s and V_{Ru} = 0.018 nm/s. Then a photoresist layer was applied for further photolithographic stripping to form the protective template of a Hall contact structure (see below). The sputtering rate was calibrated with a NTEGRA Aura atomic force microscope (AFM). To this end, single-layered films of each material used with thicknesses of approx. 50 nm were synthesized. Some sections of the films were deposited on weakly adhesive domestic alcohol marker substrates and subsequently mechanically removed from the substrates so as to produce a step for further high-accuracy film thicknesses measurements. Furthermore, for each composition the mean-square surface roughness was assessed to be approx. 0.3 nm.

The structure of the specimens was studied using X-ray diffraction on a D8 Advance diffractometer in CuK_α radiation. The studies showed that all the experimental specimens were polycrystalline and contained small fractions of amorphous structure.

Measurements of current-induced spin transport required Hall bridge structures with variable width (with narrowed sections) be formed on the specimens. The 20.5 and 0.7 mm narrow sections were synthesized using electron beam lithography on the basis of a Scios 2Dual Beam electron microscope with a Raith attachment (10 kV accelerating voltage, 0.4 nA beam current and 30 nm beam diameter). The printing was accomplished at a 180$^\times$ magnification, i.e., the exposed field area was 1×1 mm^2, the exposure step being 16 nm. The photoresist was Micro Chem PMMAA2, the irradiation dose being 125 mC/cm^2. A photoresist film was applied at a 3000 rpm speed and baked at 453.15 K for 1 min. The photoresist film thickness was approx. 300 nm. Ion beam etching was conducted with an Oxford PlasmaLab 80Plus system. Unprocessed film sections were stripped off by plasma etching from the entire specimen surfaces except the areas protected by the photoresist template. The base pressure in the chamber was $1 \cdot 10^{-3}$ Pa, the Ar gas pressure was 0.7 Pa, the plasma generator power was 400 W and the etching time was 3 min.

Electric contact templates were printed on a Suss Microtec MJB4 contact photolithographic system (Fig. 1*b*). FP-2514 positive photoresist from FRAST-M Co. was used for exposure. The photoresist was applied at a 3000 rpm speed and baked at 368.15 K for 1 min. The photoresist film thickness was ~1.5 mm. Following photoresist stripping in acetone, Hall structures with 200 long and 20 mm wide conductors were formed on the specimen surface. Electric contacts were formed by coating the specimens with another photoresist layer in which

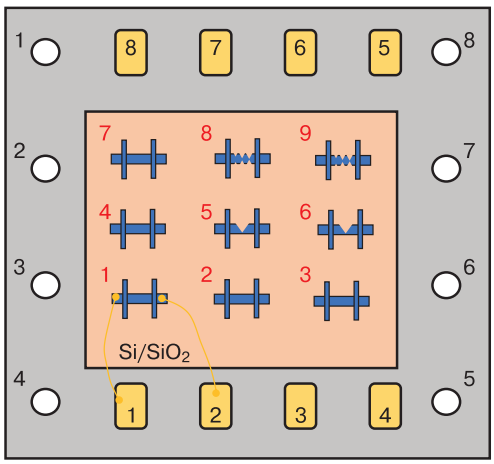

Figure 2. Schematic of final on-chip specimen with nine Hall contact film structures

electric contact pads were formed by photolithography. The surface adhesion of the electric microcontacts was improved by applying a Ti/Au layer in a custom-made thermal deposition plant. A current of ~30 A was sequentially passed through heating coils inside which a titanium and gold weighed dose was placed. Titanium was initially deposited from solid state for 20 s to form a 5–15 nm thick film for gold adhesion improvement. The Au weighed dose was sputtered completely: sputtering of a 70 mg gold dose produced a ~60 nm thick film on the specimen surface. The sputtering chamber had an exhaust cart with a turbomolecular vacuum pump developing a pressure of $\sim 0{,}1 \cdot 10^{-3}$ Pa.

As a result, single-layered films and Hall-shaped contact film structures were synthesized. The final film structure specimens formed on a silicon chip (substrate) had 4×4 mm^2 dimensions and were then separated using ultrasonic welding with ~20 mm diam. aluminum wires to form a wedge-to-wedge arrangement. The welded contact diameter was ~60 mm. Thus, each chip specimen contained nine Hall-type structures having different conductive contact thicknesses (Type 1: 20 mm, Type 2: 5 mm and Type 3: 2 mm, see Fig. 2). Each Hall-type structure had six contacts: two at the edges of the current conductor and four transverse contacts for measuring the longitudinal and lateral potential drops under bias. Thin copper wires were soldered to the chip leads for easy connection.

3. Results and discussion

The magnetic properties (magnetization state, coercive force, magnetic anisotropy energy etc.) were studied for continuous films using vibration magnetometry (Lake Shore 7401VSM) in up to 3 T fields at 78–800 K. The magnetometer holder allowed measuring the specimen orientation relative to the magnetic field direction. Hysteresis loops were taken for each film in the easy magnetization axis (EMA) direction which for all the test specimens was perpendicular to the film plane, and along the

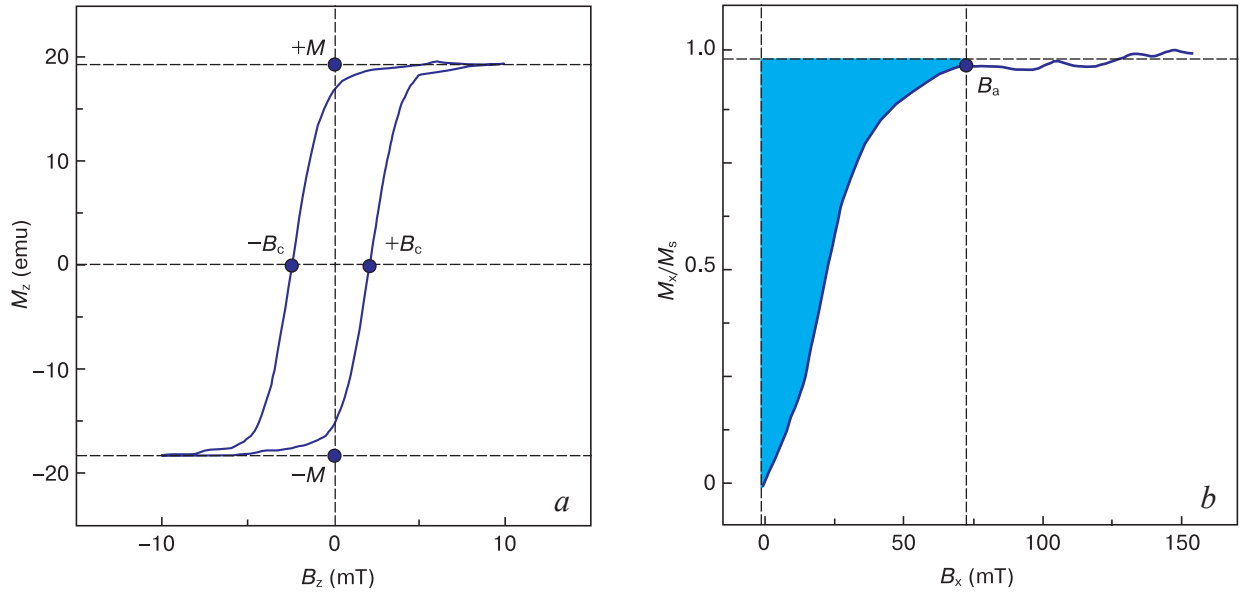

Figure 3. (*a*) Magnetic hysteresis loop for continuous film with magnetic field perpendicular to the film plane and (*b*) half of hysteresis loop for continuous film with magnetic field within the film plane

hard magnetization direction, i.e., within the film plane. The former curves were used for calculating the saturation magnetization and the coercive force, and the latter ones, for determining the magnetic anisotropy energy.

Figure 3*a* shows a typical magnetic hysteresis loop for a continuous film with field applied along the easy magnetization axis, i.e., perpendicularly to the film. The loop exhibits four typical points: the positive and negative magnetic inductions B_c at which the magnetization is zero and the positive and negative magnetizations M. The mean magnetic induction B_c characterizes the coercive force and the mean magnetic moment M_0 shows the saturation magnetization. The saturation magnetization M_s, i.e., the specific magnetic moment per unit volume, is calculated based on the accurate measurement of the film surface area S on a specimen photograph superimposed with millimeter grid paper. Knowing the magnetic layer thickness t_F one can calculate the saturation magnetization M_s using the following formula:

$$M_s = \frac{M_0 \cdot 10^{-3}}{St_F}. \quad (1)$$

Figure 3*b* shows a typical magnetization curve for a continuous film measured perpendicular to the EMA, i.e., within the film plane. Since the magnetic moment can be measured with a higher accuracy upon remagnetization along the EMA, the curve was reduced to the units of M_n, and the saturation magnetization M_s for the calculation was taken from the previous calculation. The area between the coordination axis and the magnetization curve is proportional to the magnetic anisotropy energy which can be thus calculated using the following formula [25]:

$$K_u = M_s \int_0^1 B_x \mathrm{d}M_n. \quad (2)$$

Table 1. Magnetic and electrical characteristics of heavy metal/ferromagnetic multilayered samples

Parameter	Specimen # (Composition)			
	#1 (Ru/Co/Ru)	#2 (Ru/Co/Ru/W)	#3 (Pt(5)/Co/MgO/Pt)	#4 (Pt(15)/Co/MgO/Pt)
M_s (10^6 A/m)	0.51	0.49	0.80	0.87
H_a (mT)	450	150	600	590
K_u (10^5 J/m^3)	0.43	0.13	1.67	1.77
H_C (mT)	2.9	2.2	74	75
ρ (10^{-7} Ohm·m)	5.1	12.0	4.7	4.6
I (mA) (for different structures):				
Type 1	25	25	22	60
Type 2	5	5	4	12
Type 3	0.5	0.5	0.3	0.6

Note. H_a: anisotropy field; H_c: coercive force; ρ: electrical resistivity; I: critical current for different types of Hall structures.

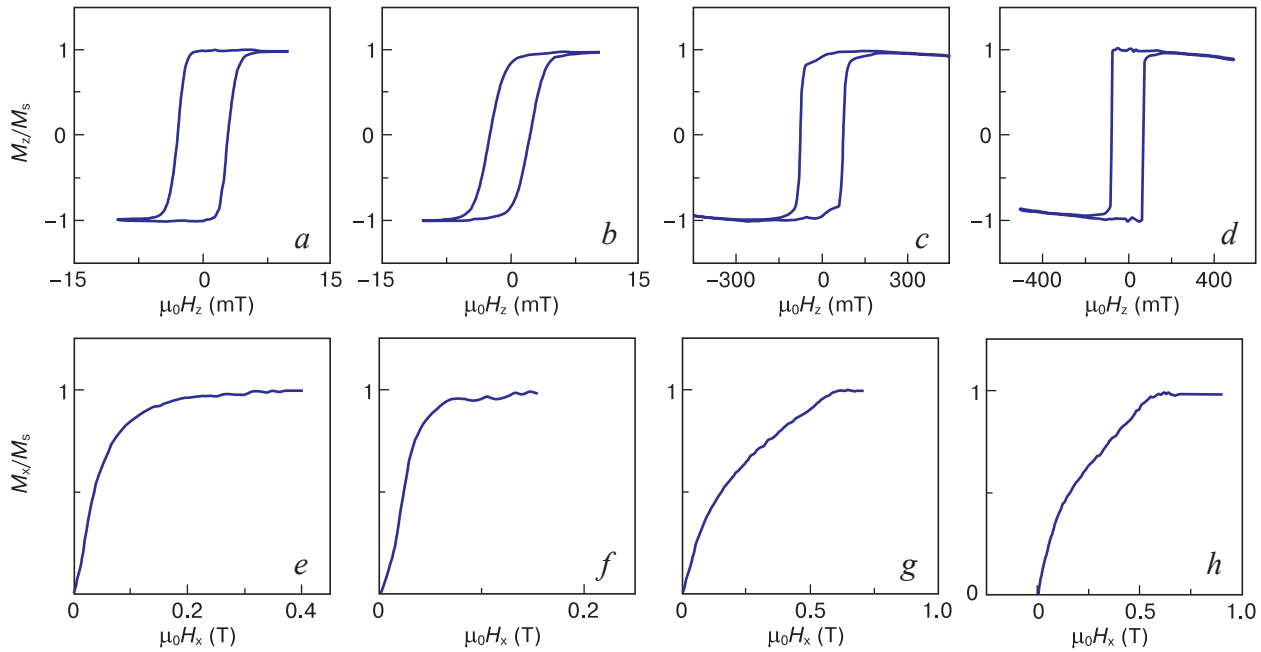

Figure 4. Magnetic hysteresis loop for magnetic field orientation (*a*–*d*) perpendicular and (*e*–*h*) along the film plane: (*a*, *e*) Ru/Co/Ru; (*b*, *f*) Ru/Co/Ru/W; (*c*, *g*) Pt(5)/Co/MgO/Pt; (*d*, *h*) Pt(15)/Co/MgO/Pt

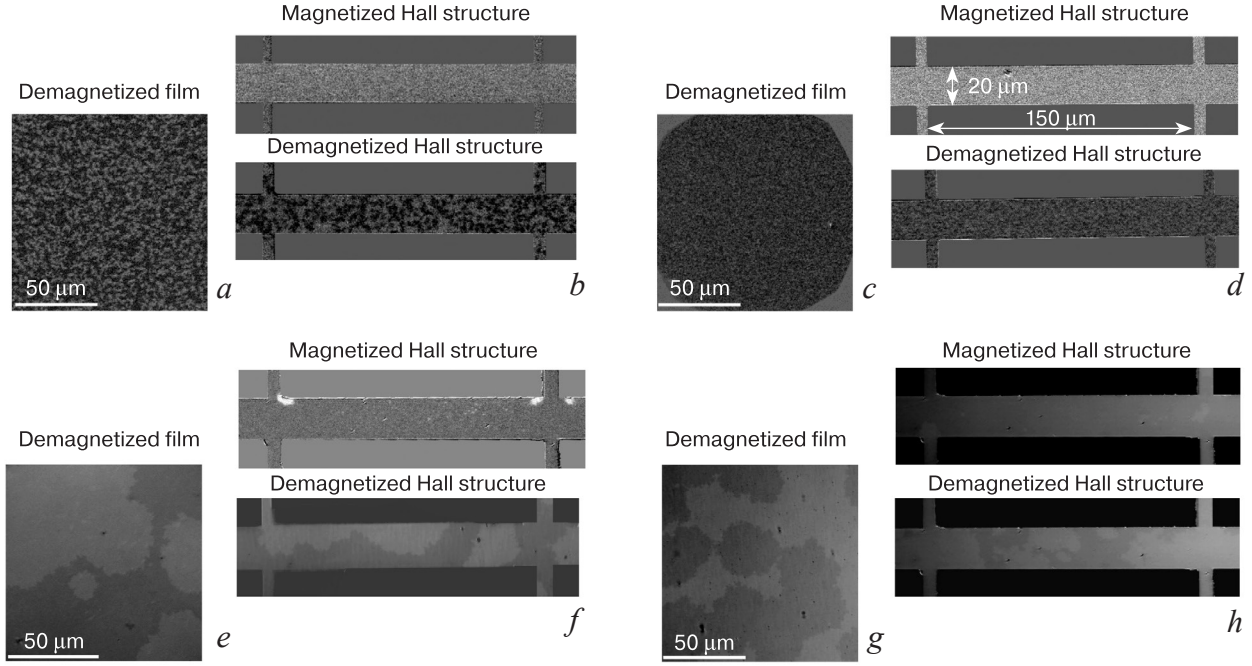

Figure 5. Magnetooptic Kerr microscopy of test films: *(a*, *b)* Ru/Co/Ru; (*c*, *d*) Ru/Co/Ru/W (the typical scale of the structure in the drawings is indicated by red numbers); (*e*, *f*) Pt(5)/Co/MgO/Pt; (*g*, *h*) Pt(15)/Co/MgO/Pt. (*a*, *c*, *e*, *g*) continuous films in demagnetized state; (*b*, *d*, *f*, *h*) Hall-shaped films with and without field

The field at which the magnetization is saturated in the plane was accepted as the anisotropy field B_a. The latter parameter was subsequently used for analysis of magnetic anisotropy in the film.

The EMA direction for all the test specimens was perpendicular to the film plane, i.e., the specimens had perpendicular magnetic anisotropy which meets the requirements. The hysteresis loop width, the coercive force and the anisotropy and magnetization fields are controlled by the parameters of the structures, primarily, by the thicknesses and combination of the layers. The minimum hysteresis loop width and hence coercive force were obtained for the Ru/Co specimens (Specimens 1 and 2, see Table 1). For the Pt/Co structures (Specimens 3 and 4) the above parameters were almost one order of magnitude higher, the hysteresis loop being almost rectangular. Additional deposition of a top nonmagnetic metallic W layer onto the Ru/Co film did not affect the saturation

magnetization and the coercive force of Specimen 2 but substantially reduced the anisotropy field and magnetic anisotropy energy (Fig. 4).

The remagnetization processes were visualized and the domain sizes in the continuous film specimens and the contact structure specimens were assessed from Kerr microscopy data (Evico Magnetics). The microscope allowed visualization of magnetization switching in the test objects (domains) sized up to 800 nm. The Kerr microscope specimen holder had two electric magnets for simultaneous generation of two magnetic fields, i.e., within (±400 mT) and perpendicularly (±120 mT) to the film plane. Figure 5 illustrates the magnetic structure of the film in a demagnetized state and the Hall structure-shaped films with and without an external magnetic field.

The specific electrical resistivity of the test contact nanostructures was ~10^{-7} Ohm·m (Table 1). The critical current in the structures was 0.5 to 60 mA. The differences in the electrical resistivities and in the critical currents (above which the Hall bridge is destroyed) for the Hall contact films originates, along with the different compositions and structure configuration, from the fact that currents in those systems pass not only through the HM layer but also through the FM one and other auxiliary films. One should therefore take into account shunting in the design of the test structures for studying various current-induced processes. Nevertheless, simple Kirchhoff rule assessments yield a maximum current density of ~10^{11} A/m^2 for the narrow structure section. This suggests that the required magnitude of current-induced effects (Oersted fields) on the magnetic structure of ferromagnetic materials is achievable [26, 27] and one can therefore use the test specimens for both the spintronics and spin-orbitronics applications.

4. Conclusion

Multilayered polycrystalline HM/FM Ru(10)/Co(0,8)/Ru(2), Ru(10)/Co(0,8)/Ru(2)/W(4), Pt(5)/Co(0,8)/MgO(2)/Pt(2) and Pt(15)/Co(0,8)/MgO(2)/Pt(2) metallic structures were synthesized using magnetron sputtering. Analysis of the magnetic properties of the structures showed that the specimens exhibit perpendicular magnetic anisotropy and low-field domain structure switching. Different configurations of Hall contact structures were synthesized using lithographic techniques with Hall bridge thicknesses of 0.7–2 mm. The critical current and current density of the structures were assessed. The synthesized specimens can be used for studies of current-induced effects on the magnetic structure of ferromagnetic materials and the formation of different topological spin textures, as well as for the electric control of spins in HM/FM structures. Results of such experiments are indispensable for the improvement of strong spin-orbital interaction structure technologies.

Acknowledgements

The work was supported by the Russian Science Foundation grant No. 21-72-20160 (https://rscf.ru/en/project/21-72-20160). The Authors are also grateful to the Joint Use Center of the Far East Federal University.

References

1. Tumanski S. Thin film magnetoresistive sensors. Bristol; Philadelphia: Inst. of physics publ., Cop; 2001. 433 p. https://doi.org/10.1887/0750307021
2. Fert A. Nobel lecture: Origin, development, and future of spintronics. *Reviews of Modern Physics*. 2008; 80: 1517. https://doi.org/10.1103/RevModPhys.80.1517
3. Naumova L.I., Milyaev M.A., Zavornitsin R.S., Pavlova A.Y., Maksimova I.K., Krinitsina T.P., Chernyshova T.A., Proglyado V.V., Ustinov V.V. High-sensitive sensing elements based on spin valves with antiferromagnetic interlayer coupling. *The Physics of Metals and Metallography*. 2019; 120: 653–659. https://doi.org/10.1134/S0031918X1907007X
4. Cardoso S., Leitao D.C., Dias T.M., Valadeiro J., Silva M.D., Chicharo A., Silverio V., Gaspar J., Freitas P.P. Challenges and trends in magnetic sensor integration with microfluidics for biomedical applications. *Journal of Physics D: Applied Physics*. 2017; 50(21): 213001. https://doi.org/10.1088/13616463/aa66ec
5. Epitaxial growth of complex metal oxides. Koster G., Huijben M., Rijnders G. (eds.). Elsevier; 2015. 479 p. https://doi.org/10.1016/C20180026596
6. Scheunert G., Heinonen O., Hardeman R., Lapicki A., Gubbins M., Bowman R.M. A review of high magnetic moment thin films for microscale and nanotechnology applications. *Applied Physics Reviews*. 2016; 3: 011301. http://dx.doi.org/10.1063/1.4941311
7. Chernyshova T.A., Milyaev M.A., Naumova L.I., Proglyado V.V., Bannikova N.S., Maksimova I.K., Petrov I.A., Ustinov V.V. Magnetoresistive sensitivity and uniaxial anisotropy of microstrips of spin valves with a synthetic antiferromagnet. *Physics of Metals and Metallography*. 2017; 118: 415–420. https://doi.org/10.1134/S0031918X17050040
8. Fukuzawa H., Iwasaki H., Koi K., Sahashi M. Soft magnetic characteristics of an ultrathin CoFeNi free layer in spin-valve films. *Journal of Magnetism and Magnetic Materials*. 2006; 298(1): 65–71. https://doi.org/10.1016/j.jmmm.2005.03.010
9. Svalov A.V., Sorokin A.N., Savin P.A., García-Arribas A., Fernández A., Vas'kovskiy V.O., Kurlyandskaya G.V. Co/Cu/Co pseudo spin-valve system prepared by magnetron sputtering with different argon pressure. *Key Engineering Materials*. 2015; 644: 211–214. https://doi.org/10.4028/www.scientific.net/KEM.644.211

10. Lau J.W., Shaw J.M. Magnetic nanostructures for advanced technologies: fabrication, metrology and challenges. *Journal of Physics D: Applied Physics*. 2011; 44(30): 303001. https://doi.org/10.1088/00223727/44/30/303001
11. Parkin S., Hayashi M., Thomas L. Magnetic domain-wall racetrack memory. *Science*. 2008; 320(5873): 190–194. https://doi.org/10.1126/science.1145799
12. Ummelen F., Swagten H., Koopmans B. Racetrack memory based on inplane-field controlled domain-wall pinning. *Scientific Reports*. 2017; 7(1): 833. https://doi.org/10.1038/s41598-017-00837-x
13. Jungfleisch M.B., Zhang W., Hoffmann A. Perspectives of antiferromagnetic spintronics. *Physics Letters, Section A: General, Atomic and Solid State Physics*. 2018; 382(13): 865–871. https://doi.org/10.1016/j.physleta.2018.01.008
14. Wang F., Bürgler D.E., Adam R., Parlak U., Cao D., Greb C., Heidtfeld S., Schneider C.M. Magnetization relaxation dynamics in $[Co/Pt]_3$ multilayers on pico- and nanosecond timescales. *Physical Review Research*. 2021; 3(3): 033061. https://doi.org/10.1103/PhysRevResearch.3.033061
15. Rinkevich A.B., Perov D.V., Kuznetsov E.A., Milyaev M.A., Romashev L.N., Ustinov V.V. Microwave penetration through $(Fe_{0.82}Ni_{0.18})$/V superlattices. *Journal of Magnetism and Magnetic Materials*. 2020; 493: 165700. https://doi.org/10.1016/j.jmmm.2019.165700
16. Manchon A., Belabbes A. Chapter One – Spin-orbitronics at transition metal interfaces. *Solid State Physics*. 2017; 68: 1–89. https://doi.org/10.1016/bs.ssp.2017.07.001
17. Bogdanov A.N., Yablonskii D.A. Thermodynamically stable "vortices" in magnetically ordered crystals. The mixed state of magnets. *Zhurnal éksperimental›noĭ i teoreticheskoĭ fiziki = The Journal of Experimental and Theoretical Physics*. 1989; 95(1): 178.
18. Fert A., Reyren N., Cros V. Magnetic skyrmions: advances in physics and potential applications. *Nature Reviews Materials*. 2017; 2(7): 17031. https://doi.org/10.1038/natrevmats.2017.31
19. Wiesendanger R. Nanoscale magnetic skyrmions in metallic films and multilayers: a new twist for spintronics. *Nature Reviews Materials*. 2016; 1(7): 16044. https://doi.org/10.1038/natrevmats.2016.44
20. Everschor-Sitte K., Masell J., Reeve R.M., Kläui M. Perspective: Magnetic skyrmions – Overview of recent progress in an active research field. *Journal of Applied Physics*. 2018; 124(24): 240901. https://doi.org/10.1063/1.5048972
21. Nagaosa N., Tokura Y. Topological properties and dynamics of magnetic skyrmions. *Nature Nanotech*. 2013; 8: 899–911. https://doi.org/10.1038/nnano.2013.243
22. Sinova J., Valenzuela S.O., Wunderlich J., Back C.H., Jungwirth T. Spin Hall effects. *Reviews of Modern Physics*. 2015; 87(4): 1213–1260. https://doi.org/10.1103/RevModPhys.87.1213
23. Heinonen O., Jiang W., Somaily H., Te Velthuis S.G., Hoffmann A. Generation of magnetic skyrmion bubbles by inhomogeneous spin Hall currents. *Physical Review B*. 2016; 93: 094407. https://doi.org/10.1103/PhysRevB.93.094407
24. Jiang W., Chen G., Liu K., Zang J., Te Velthuis S.G., Hoffmann A. Skyrmions in magnetic multilayers. *Physics Reports*. 2017; 704: 1–49. https://doi.org/10.1016/j.physrep.2017.08.001
25. Vonsovskiĭ S.V. Magnetism. New York: J. Wiley; 1974. 1256 p.
26. Manchon A., Železný J., Miron I. M., Jungwirth T., Sinova J., Thiaville A., Garello K., Gambardella P. Current-induced spin-orbit torques in ferromagnetic and antiferromagnetic systems. *Reviews of Modern Physics*. 2019; 91(3): 035004. https://doi.org/10.1103/RevModPhys.91.035004
27. Stebliy M.E., Kolesnikov A.G., Ognev A.V., Davydenko A.V., Stebliy E.V., Wang X., Han X., Samardak A.S. Advanced Method for the reliable estimation of spin-orbit-torque efficiency in low-coercivity ferromagnetic multilayers. *Physical Review Applied*. 2019; 11(5): 054047. https://doi.org/10.1103/PhysRevApplied.11.054047